

3D imaging of geofluid by wideband magnetotellurics

OGAWA, Yasuo^{1*} ; ICHIKI, Masahiro² ; KANDA, Wataru¹

¹Volcanic Fluid Research Center, Tokyo Institute of Technology, ²Graduate School of Science, Tohoku University

Magnetotelluric measurements have been conducted over the five years in the central part of NE Japan arc surrounding the Naruko Volcano with approximately 3km grid. Over 200 sites were used for modeling the crustal resistivity structure in detail. Full impedance tensors for 8 periods were used for inversion. To alleviate the computational load, first four short periods were used to image upper crustal features and the resultant model was used for a prior model for another set of inversions with longer 4 periods.

The obtained model show the crustal conductor underneath the Mukaimachi caldera and Sanzugawa caldera. Seismic tomography shows low S-wave velocity for both, however, the resistivity image show clear low resistivity for Mukaimachi Caldera, but not for Sanzugawa Caldera. This difference may be due to the salinity of the fluids underlying the volcanic regions.

Keywords: geofluid, magnetotellurics, resistivity, 3d

Three dimensional electrical conductivity model in the subduction zone beneath north-eastern Japan

ICHIKI, Masahiro^{1*} ; OGAWA, Yasuo² ; KAIDA, Toshiki¹ ; DEMACHI, Tomotsugu¹ ; HIRAHARA, Satoshi¹ ; HONKURA, Yoshimori² ; ICHIHARA, Hiroshi³ ; KANDA, Wataru² ; KONO, Toshio¹ ; KOYAMA, Takao⁴ ; MATSUSHIMA, Masaki⁵ ; NAKAYAMA, Takashi¹ ; SUZUKI, Shu'ichi¹ ; TOH, Hiroaki⁶ ; UYESHIMA, Makoto⁴

¹Grad. School of Sci., Tohoku University, ²VFRC, Tokyo Institute of Technology, ³IFREE, JAMSTEC, ⁴ERI, The University of Tokyo, ⁵Grad. School of Sci. & Eng., Tokyo Tech, ⁶Grad. School of Sci., Kyoto University

Our final goal is to infer a geofluid map (GFM) from both of the seismological (seismic velocity, V_p/V_s , Q etc.) and electrical conductivity structures in the wedge mantle of subduction zone beneath northeastern Japan. While plenty of high-resolution three dimensional (3-D) seismic tomographic images has been revealed there, none of 3-D electrical conductivity distribution model, of which the resolution is comparative to those of seismic tomography, has been proposed in terms of wedge mantle in subduction zones. Here, we show a high-resolution 3-D electrical conductivity distribution model in the wedge mantle beneath northeastern Japan used as input of GFM.

We carried out long-period MT observation using the state-of-the-art equipments, LEMI-417 and NIMS. The total 72 site observation has been completed. To remove tilt changes, baseline steps and drifts of fluxgate magnetometers, we first subtracted magnetic field variations to which a median filter was applied, from raw data. The horizontal coordinate of magnetic field data in each site was rotated before the response calculation such that the declination of the averaged horizontal component should be consistent with the 2010 absolute geomagnetic observation map provided by Geospatial Information Authority of Japan. We used the BIRRP processing code (Chave and Thomson, 2004) to estimate MT responses and have successfully retrieved them up to 61440 seconds in period.

The MT impedance responses were inverted into 3-D electrical conductivity model using WSINV3D (Siripunvaraporn et al, 2005), the data-space Occam inversion method. The all input data error floor was assigned to be 10 percent. We investigated the optimal reference model with trial and errors. The test model was (1) uniform models, (2) layered models and (3) layered models with subducting slab models. The best RMS in each reference model was (1) 2.81, (2) 2.71 and (3) 2.48, respectively. Hence, we adopted the reference model of the layered model with subducting slab.

The conductivity profiles normal to the trench axis in higher latitude than N 39 degrees delineate conductive region on the subducting slab, and the conductive region is raised just beneath the central range of northeastern Japan (Ou-backbone range). This electrical image is well consistent with that obtained by the seismic tomographic model. On the other hand, a profile in lower latitude than N 39 degrees reveals that the conductive region is overturned towards backarc. The top of the overturned conductive body coincides with Gassan Volcano location, one of the outstanding backarc volcanism. However, Chokai Volcano, another distinctive backarc volcanism has no subsurface conductive root originated from deep upper mantle. The overturned mantle convection image is not found in the seismic tomographic image.

S-wave attenuation on the western side of Nankai subduction zone: implications for geofluid distribution and dynamics

TAKAHASHI, Tsutomu^{1*} ; OBANA, Koichiro¹ ; YAMAMOTO, Yojiro¹ ; NAKANISHI, Ayako¹ ; KODAIRA, Shuichi¹ ; KANEDA, Yoshiyuki¹

¹JAMSTEC

One major cause of seismic wave attenuation is the presence of fluid in rocks. In this study, we estimated the attenuation structure in southwestern Japan and western Nankai trough by applying the attenuation tomography that takes account of apparent amplitude attenuation due to multiple forward scattering [Takahashi, 2012]. Because the estimated attenuation $1/Q$ in our tomographic study was much larger than $1/Q$ due to wide-angle scattering, our estimated $1/Q$ is composed mainly the intrinsic $1/Q$.

High $1/Q$ ($>1/500$ at 4-8 Hz) was imaged beneath the Quaternary volcanoes. The highest attenuation ($1/Q \sim 1/250$ at 4-8 Hz) distributes beneath the Beppu-Shimabara rift zone at 40-60km depth. Beneath this rift zone, $1/Q$ becomes larger as depth increases. Random inhomogeneities in this zone are relatively strong at 0-40 km depth; whereas at 40-60 km depth random inhomogeneities are almost comparable to those in non-volcanic area. Meanwhile, in northeastern Japan, uppermost mantle beneath the volcanoes shows strong inhomogeneities and high attenuation. Apparent attenuation at the uppermost mantle beneath the Quaternary volcanoes is high in both study areas, but relative contributions of scattering and intrinsic attenuation differ between northeastern Japan and the Beppu-Shimabara rift zone. If we consider random inhomogeneities and $1/Q$ in other areas, the weak random inhomogeneities and high $1/Q$ beneath this rift zone suggest that random inhomogeneities due to the presence of igneous rocks are not significant, and that any magma inclusions are too small to excite S-wave scattering at 4-32 Hz.

At off Shikoku region, moderate $1/Q$ ($1/800 \sim 1/1000$ at 4-8 Hz) is imaged at 0-20 km depth. This moderate $1/Q$ is estimated as $1/Q(f) \sim 10^{-2.5} f^{-0.5}$. Similar moderate attenuation can be found beneath the south of Shikoku at 20-40km, beneath the northern edge of Shikoku at 40-60km depth, and beneath Chugoku area at 40-60km depth. From geometry models of subducting Philippine Sea plate, most of the moderate $1/Q$ zone is located in and around the oceanic crust of subducting Philippine Sea plate except beneath Chugoku region. In this area, Shelly et al. [2006] pointed out fluid existence in the oceanic crust by estimating V_p/V_s structure. This correspondence implies this moderate $1/Q$ reflects fluid in the subducting slab. If we suppose that $1/Q$ of P- and S-wave have the same frequency dependences and that random inhomogeneities of P- and S-wave has the same scale dependences, we can show possible cases of fluid flow induced by the passage of low frequency seismic waves (<1 Hz) by applying a theoretical model of wave attenuation in saturated porous random media [Muller and Gurevich, 2005]. As a phenomenon suggesting such fluid flow by lower frequency seismic wave, triggering of non-volcanic tremors by surface waves passing has been observed [e.g., Miyazawa and Brodsky, 2008]. Even though we further need P-wave studies for detailed examination of this topic, it is likely that random inhomogeneity, intrinsic at 4-32 Hz and triggered tremors can be used to investigate medium properties and fluid dynamics.

Seismic activity near the Moriyoshi-zan volcano in northeastern Japan: Implications for geofluid migration

KOSUGA, Masahiro^{1*}

¹Graduate School of Science and Technology

The 2011 Off the Pacific coast of Tohoku (Tohoku-oki) Earthquake caused increased seismicity in many inland areas. A seismic cluster that occurred north of the Moriyoshi-zan volcano in the Akita prefecture of the Tohoku District is of interest in light of contribution of geofluids to seismic activity. We observed a seismic cluster characterized by the migration of seismicity, reflected/scattered phases, and deep low-frequency earthquakes. We relocated hypocenters by using the data of temporal observation and by using the Double-Difference location technique, which increased the depth accuracy. We interpreted the spatiotemporal variation of the hypocenters in the most active cluster by estimating the migration of pore fluid pressure. The hydraulic diffusivity of the cluster was in the range of 0.01-1.0 m²/s, and increased with time, implying that the migration of hypocenters accelerated after a pathway for fluids was formed by the fracturing of the wallrock that produced the initial stage of seismic activity. A prominent feature of the seismograms is a reflected/scattered phase observed at stations around the volcano. We have interpreted the phase as S-to-S scattered waves and estimated the location of scatterers using a back-projection method. The scatterers are located about 5 km northwest of the Moriyoshi-zan volcano and at an approximate depth of 13 km. The Moriyoshi-zan area is one of the source areas of deep low-frequency earthquakes that have previously been interpreted as events generated by the migration of geofluids. The depth of scatterers is close to the upper limit of the depth at which low-frequency earthquakes occur. Thus, we regard the observed scatterers to be a reservoir of geofluid that came from the uppermost mantle accompanying contemporaneous low-frequency earthquakes. The geofluid reservoir is the probable source of overpressurized fluid that induces the migration of seismicity in the upper crust. A time delay in seismic activity from the Tohoku-oki Earthquake was considered as the time needed to migrate across a gap between the reservoir and the earthquake cluster with a hydraulic diffusivity comparable to that observed for the initial stage of seismicity, i.e., fracturing of the wallrock.

Keywords: The 2011 Off the Pacific coast of Tohoku Earthquake, triggered seismicity, hypocenter migration, scattering, geofluid

Is H₂O-NaCl fluid enough to explain high electrical conductivity in the earth's crust?

SAKUMA, Hiroshi^{1*} ; ICHIKI, Masahiro²

¹National Institute for Materials Science, ²Tohoku University

Old continental crust has a high electrical conductivity layer at 20 to 30 km in depth [1]. Presence of aqueous fluids is a plausible hypothesis for explaining the high conductivity zone [2]. Therefore the electrical conductivities of aqueous fluids under high pressure (P), temperature (T) conditions should be investigated in order to evaluate the hypothesis. The phases of water and aqueous NaCl solutions at the P - T conditions of the Earth's crust correspond from liquid to supercritical states.

Experimental approaches to measure the electrical conductivities at high P , T and salt concentration (c) conditions are limited and the data at $P < 400$ MPa, $T < 1073$ K and $c < 0.6$ wt% for aqueous NaCl solutions is only available [3]. Classical molecular dynamics (MD) simulations are useful to obtain the electric conductivities at high P , T and c conditions and for understanding the underlying mechanism controlling the conductivities.

We used the flexible and induced point charge (FIPC) H₂O model [4] for MD simulations of aqueous NaCl solution. The technical details of the model and computational methods are explained in the literature [4]. The unit cell contained 2222 H₂O and 4 NaCl, 2035 H₂O and 22 NaCl, and 2035 H₂O and 66 NaCl for $c = 0.6, 3.4,$ and 9.6 wt% NaCl solutions, respectively.

The isotherms indicate that the conductivity increases with increasing pressures and saturated at high pressures. The conductivity decreased with increasing temperature. This behavior may seem to be strange, since the ionic mobility should be high at high temperatures. This can be explained by the mixed effects of the change of (i) the density, (ii) ionic mobility, and (iii) dielectric constant of water as discussed in Quist and Marshall (1968) [3]. We concluded that the change of the conductivity of H₂O-NaCl fluids along with a geotherm model can explain one order of the increased magnitude at the high conductivity layer in depth, but more change observed by the Magnetotelluric method should be explained by the additional mechanism such as the connectivity of the fluids and the conductivity of H₂O-CO₂ fluids.

References

- [1] T. J. Shankland and M. E. Ander (1983) *J. Geophys. Res.* **88** 9475-9484.
- [2] B. E. Nesbitt (1993) *J. Geophys. Res.* **98** 4301-4310.
- [3] A. S. Quist, and W. L. Marshall, (1968) *J. Phys. Chem.* **72** 684-703.
- [4] H. Sakuma, M. Ichiki, K. Kawamura and K. Fuji-ta (2013) *J. Chem. Phys.* **138** 134506.

Keywords: salt water, electrical resistivity, supercritical fluid, molecular dynamics, static dielectric constant

Connectivity of cracks and pores in a granitic rock

WATANABE, Tohru^{1*} ; HIGUCHI, Akiyoshi¹ ; YONEDA, Akira²

¹Graduate school of science and engineering, University of Toyama, ²Institute for Study of Earth's Interior, Okayama University

Seismic velocity and electrical conductivity are used to map the fluid distribution in the crust. Seismic velocity reflects the contiguity of solid phases, while electrical conductivity the connectivity of fluid phases. The combination of velocity and conductivity could provide us a strong constraint on the fluid distribution. However, mapping of the fluid distribution has not been successful. The connectivity of fluid phases in rocks is poorly understood. In order to understand the connectivity of fluid phases in rocks, we have made conductivity measurements on a fluid-bearing granitic rock under various confining pressures.

Fine grained (100-500 μ m) biotite granite (Aji, Kagawa pref., Japan) was used as a rock sample. The sample is composed of 52.8% plagioclase, 36.0% Quartz, 3.0% K-feldspar, 8.2% biotite. The density is 2.66(1) g/cm³, and the porosity 0.8(1) %. The porosity was estimated from the mass of the dry and wet samples. Cylindrical samples have dimensions of 25 mm in diameter and 30 mm in length, and saturated with 0.01 mol/l KCl aqueous solution. Simultaneous measurements of elastic wave velocity and electrical conductivity were made using a 200 MPa hydrostatic pressure vessel. The pore-fluid is electrically insulated from the metal work by using plastic devices (Watanabe and Higuchi, 2013). The confining pressure was progressively increased up to 125 MPa, while the pore-fluid pressure was kept at 0.1 MPa. It took five days or longer for the electrical conductivity to become stationary after increasing the confining pressure.

Elastic wave velocities and electrical conductivity showed reproducibly contrasting changes for a small increase in the confining pressure. Elastic wave velocities increased only by 5% as the confining pressure increased from 0.1 MPa to 25 MPa, while electrical conductivity decreased by an order of magnitude. The increase in velocities is caused by the closure of cracks. Most (~80%) of the decrease in electrical conductivity occurred below the confining pressure of 5 MPa. The decrease in electrical conductivity must also be caused by the closure of cracks. The decrease in porosity was only 0.07(1) %. Such a small change in porosity caused a large change in electrical conductivity. The connectivity of fluid was maintained at least up to the confining pressure of 125 MPa. A calculation with the effective medium theory (Kirkpatrick, 1973) suggests that the fluid forms a network with small coordination number (average coordination number=2.3), and that the connectivity at higher pressures is maintained by stiff pores. More cracks are open at lower pressures to link pores, drastically increasing electrical conductivity.

Keywords: pore, crack, connectivity, granitic rock, electrical conductivity

Geometry of intergranular fluids in the mantle xenoliths: Implications for the physical properties of upper mantle

NAKAMURA, Michihiko^{1*}; OKUMURA, Satoshi¹; YOSHIDA, Takeyoshi¹; SASAKI, Osamu²; TAKAHASHI, Eiichi³

¹Graduate School of Science, Tohoku University, ²Tohoku University Museum, ³Graduate School of Science and Engineering, Tokyo Institute of Technology

Recent magnetotelluric (MT) studies have revealed that crust and uppermost mantle are less resistive than dry rocks in various localities in the world. This suggests that interconnected fluid phases present more ubiquitously than previously realized. Intergranular fluids also decrease seismic wave velocities and changes Vp/Vs ratio, thus interpretation of the seismic tomographic images largely depends on the volume fraction and geometry of the fluid phase. The conventional view on grain-scale fluid distribution is based on dihedral angle between minerals and fluids in isotropic monomineralic rocks (i.e. ideal equilibrium geometry). Natural rocks are, however, composed of anisotropic multiple phases and undergo textural adjustment to minimize interfacial and strain energy such as grain growth and dynamic recrystallization, which results in microstructural complexity. In order to understand real fluid distribution in deep-seated rocks, we conducted an X-ray CT study of xenoliths from the uppermost mantle from various localities.

The mantle xenolith samples investigated were from Ichinomegata (NE Japan), Eifel (W Germany), San Carlos (AZ, USA), Bullen Merri and Shadwell (Victoria, AU), Kilbourne Hole (New Mexico, USA), Longang-hu (NE China), Gi-rona (Spain), Lanzarote (Canary islands), and Moses Rocks (Uta, USA). The micro-focus X-ray CT imaging was performed using Comscantecno ScanXmate-D160TSS105 in Tohoku University Museum with a tube voltage of 100 – 130 kV and current of 90 – 120 mA. The voxel size was typically 43 – 73 μm^3 . The 3-D image analysis was carried out with a software package Slice[1].

All the observed spinel lherzolite and Harzburgite xenoliths contained up to a few vol% of intergranular pores, indicating that the rocks were saturated with a free-fluid phase. The imaged pore fluids are typically polyhedral and tens – hundreds of micrometers in scale; this suggests that they were formed via coalescence of smaller pore fluids. The fluids are localized in interphase boundaries (between different mineral phases), while most of the monomineralic triple junctions lack pore fluids. All these characteristics are consistent with the results of grain-growth experiments in a fluid-bearing bimineralic system[2]; in other words, the role of interfacial energy anisotropy and grain growth are crucial in determining fluid distribution in nature. In the ellipsoid approximation, the 3-D shape of the intergranular fluids show deformed rugby-ball shape with aspect ratios larger than those of the equilibrium fluid geometry determined by the dihedral angle[3]. The geometry, distribution and thus connectivity of fluids cannot be assessed simply from dihedral angles.

The results of CT imaging suggest that no pervasive grain-scale fluid interconnection is established in the uppermost mantle. To explain the observed low electrical resistivity in the mantle which does not undergo partial melting, concentration (localization) and interconnection of CHO fluids in a larger spacing, such as in meter-scale shear zones should be necessary. Given the observed geometry of the inter-granular fluids, their effects on Vp/Vs ratio is limited.

References: [1] Nakano et al. <http://www-bl20.spring8.or.jp/slice/> (2006). [2] T. Ohuchi and M. Nakamura J. Geophys. Res. 111, B01201, doi: 10.1029/2004JB003340 (2005). [3] Y. Takei JGR 107 (B2) doi:10.1029/2001JB000522 (2002).

Keywords: mantle xenoliths, rock microstructure, elastic wave velocity, electrical resistivity, grain growth

Ultra-fine textures along grain boundaries in nominally fresh mantle xenoliths

MURATA, Masami^{1*} ; UEMATSU, Katsuyuki² ; YAMAMOTO, Takafumi³ ; TANI, Kenichiro⁴ ; SHUKUNO, Hiroshi⁵ ; MIZUKAMI, Tomoyuki¹ ; MORISHITA, Tomoaki¹

¹Kanazawa Univ., ²Marine Works Japan LTD., ³Hiroshima Univ., ⁴JAMSTEC, ⁵non party

It is important for the evolution of the Earth to understand the role of grain boundaries during melts/fluids migrations in mantle peridotites. There are, however, very limited numbers of studies on grain boundaries in natural samples, although many experimental and theoretical approaches have been carried out (e.g., Drury and Fitz Gerald, *Geophys. Res. Lett.*, 1996; Hiraga et al., *Nature*, 2004).

We focus on nanoscale microstructures of crystal surface (grain boundary) in “ nominally fresh ” peridotite xenoliths from the San Carlos, USA, which is one of the most famous localities of peridotite xenolith in the world. Thin amorphous films along grain boundaries were already reported in some San Carlos xenoliths (Wirth, *Contrib. Mineral. Petrol.*, 1996).

We recovered mineral grains with a selfFrag at the Japan Agency for Marine-Earth Science and Technology (JAMSTEC) in order to minimize mechanical damages during mineral separations. We observed multiple grains of peridotite xenoliths using a high-resolution electron microscope (FE-SEM) at JAMSTEC.

Microstructures of crystal surface of these peridotite xenoliths are classified as follows. (1) over micron scale structures such as moth-eaten structures, vermicular structures, automorphic crystals and etch pits. (2) submicron scale structures. It is interesting to note that (2) submicron scale structures are frequently observed on (1) over micron scale structures. These textures suggest that microstructures were developed by several stages. We analysed on the surface of these textures using a micro-Raman and SEM-EDS techniques. We are also planning to perform transmission electron microscope, combined with chemical analyses in order to identify the surface materials that constrain P-T conditions and fluids for the formation of these textures.

Keywords: peridotite xenolith, Microstructures, TEM, grain boundary, fluids

Elemental transport under lower-middle crustal condition: example from hydration of basic schist, Sanbagawa belt, Japan

UNO, Masaaki^{1*}; NAKAMURA, Hitomi²; IWAMORI, Hikaru³

¹Graduate School of Environmental Studies, Tohoku University, ²Department of Earth and Planetary Sciences, Tokyo Institute of Technology, ³Geochemical Evolution Research Program, Japan Agency for Marine-Earth Science and Technology

To constrain the behavior of geofluids under the lower to middle crustal conditions, hydration reactions and trace element and Sr-Nd-Pb isotopic compositions of basic schists in the Cretaceous Sanbagawa metamorphic belt, a typical regional metamorphic belt in the circum-Pacific orogeny, have been investigated based on the observations of thin-sections and outcrops. The basic schists have undergone significant hydration from 0.8 GPa, 550 °C to 0.3 GPa, 400 °C during decompression towards the surface at the final stage of metamorphism. High-field-strength and rare-earth element compositions of the basic schists, as well as the Sr-Nd-Pb isotopic ratios, are different among three mineral zones with different peak P-T metamorphic conditions; the basic schists in the low-grade chlorite zone shows N-MORB-like compositions whereas those in the higher-grades, garnet and oligoclase-biotite zones, show more enriched compositions (E-MORB-like). On the other hand, there is a common feature to all the metamorphic zones; the enrichment degree of some group of elements (e.g., large-ion lithophile elements) relative to high-field-strength and heavy-rare-earth elements is proportional to loss on ignition that approximately measures the bulk rock H₂O content. This correlation suggests that Li, B, K, Cr, Ni, Rb, Sr, Cs and Ba have been added to the basic schists during hydration. The addition of these elements amounts to as much as 60-80% of the bulk abundance, indicating that significant amounts of elements were transported via pervasive fluid flow, which overprinted the variation in the bulk rock compositions of the protolith. The estimated compositions of hydration fluid show high concentrations in large-ion lithophile elements, lead and light-rare-earth elements (10-100 times denser than primitive mantle, Fig. 1) and are similar to those of the slab-derived fluids^[1] that induce arc volcanism. These elements (Cs, Rb, Ba, K, La, Ce and Pb) are thought to have been preferentially partitioned into the fluid when it was generated at depth. Such high concentrations indicate a high temperature origin of the hydration fluid, and are consistent with a model of hot slab subduction during exhumation of the Sanbagawa belt.

References:

[1] Nakamura, H., Iwamori, H., and Kimura, J.-I., 2008 *Nat. Geosci.*, **1**, 380-384

Keywords: geofluid, metamorphism, trace elements, Sr-Nd-Pb isotopes, hydration reaction, Sanbagawa metamorphic belt

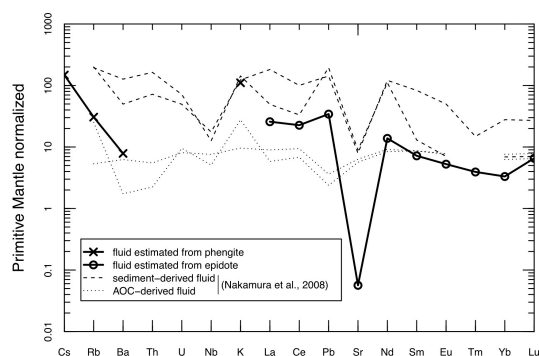


Fig. 1 Estimated compositions of the hydration fluid (solid lines). Compositions of slab-derived fluids estimated for arc volcanism (dotted lines; Nakamura *et al.*, 2008 *Nat. Geosci.*, **1**, 380-384) are shown for comparison. Note that the concentrations of LILE, Pb and LREE in the hydration fluid are in the range of slab-derived fluids.

Progress of serpentinization in the mantle wedge and its effect on the redox state

KOGISO, Tetsu^{1*} ; MIYOSHI, Akane²

¹Human Environ. Stds., Kyoto Univ., ²JX Nippon Oil & Energy Corporation

Serpentinization of peridotite in the mantle is a key process that significantly changes the physical properties of the mantle. Serpentinization also produces hydrogen, which is essential not only for the activity of microbial systems in hydrothermal fields on the seafloor, but also for controlling the oxidation state of the mantle in subduction zones. Hydrogen is generated along with the formation of magnetite during serpentinization. However, there still remains controversy about what factors promote the mineralogical reactions responsible for magnetite formation during serpentinization in natural ultramafic rocks. Recent petrologic studies have proposed that serpentinization reactions proceed via a two-stage process involving the early formation of serpentine and brucite and subsequent magnetite formation. Many studies proposed that magnetite forms by the break down of ferrous brucite promoted by the addition of aqueous silica, but others proposed that magnetite forms by the breakdown of ferrous serpentine which releases silica component. To solve this controversy, we examined a number of variably serpentinized harzburgite and dunite samples taken from the Iwanaidake ultramafic body in Kamuikotan belt, Japan (Miyoshi et al. 2014). Petrographic observations of these samples revealed that successive changes in textures, mineral chemistry, whole-rock H₂O contents, and magnetic susceptibility with the progress of serpentinization of harzburgite involved two stages: replacement of olivine by serpentine and brucite, and subsequent formation of magnetite along with more-magnesian serpentine and brucite. The later reactions occurred concurrently with serpentinization of orthopyroxene, which supplied the silica component. In serpentinized dunite, which doesn't contain orthopyroxene, serpentinization involved replacement of olivine by serpentine and brucite, and the fraction of magnetite did not increase with the progress of serpentinization. These observations, and the fact that the Iwanaidake ultramafic body originated from the forearc mantle of the Northeast Japan arc, suggest that the silica supply from serpentinization of orthopyroxene is an essential factor for the formation of magnetite during serpentinization in mantle wedge.

Our observations imply that serpentinization in the mantle wedge of subduction zone produces H₂ along with magnetite if sufficient amounts of silica component are supplied from subducting slab, which will probably occur because dehydration in subducted sediments can supply silica-rich fluids. Since H₂ is expected to exist as immiscible hydrogen-rich gas phases that coexist with H₂O fluids in normal subduction zone conditions, it will be rapidly migrate upwards owing to its very low density. Then the remaining serpentinites will become oxidized. Such oxidation associated with serpentinization would occur in the shallow part of the wedge corner where temperatures are lower than ~600 °C, but the oxidized (magnetite-bearing) serpentinite will be dragged downwards in the mantle wedge. Thus serpentinization reactions can be one of the main processes to increase the oxygen fugacity of the mantle wedge. On the other hand, the H₂ gas removed from the wedge corner will produce highly reduced fluid phases, which may result in reducing the shallowest part of the forearc mantle and the lower part of the forearc crust. This could be the cause of rare presence of metal phases in subarc peridotite.

Reference:

A. Miyoshi, T. Kogiso, N. Ishikawa, K. Mibe (2014) *American Mineralogist*, in press.

Keywords: serpentinization, hydrogen, magnetite, subduction zone, redox state

Evolution of porosity structures in a fracture during quartz vein formation

YAMADA, Ryo^{1*}; OKAMOTO, Atsushi¹; SAISHU, Hanae¹; NAKAMURA, Michihiko²; OKUMURA, Satoshi²; SASAKI, Osamu³; TSUCHIYA, Noriyoshi¹

¹Tohoku university, ²Tohoku university, ³The Tohoku university museum

Ubiquitous occurrences of quartz veins suggest that dissolution/precipitation of silica provides significant effects on the hydrological and mechanical properties within the crust. For example, a model has been proposed that fracture sealing processes control the change of pore fluid pressure and thus earthquake cycle. Previous studies on natural quartz veins have focused on estimates of P-T conditions, stress and strain fields and fluid compositions; however, details of dynamics of fluid flow and how fractures are sealed during vein formation are still unclear. In this study, we synthesized quartz veins by the hydrothermal experiments, and observed the aperture structures by using X-ray CT to clarify how aperture structures evolve during vein formation.

We conducted the hydrothermal flow-through experiments for quartz precipitation from Si-supersaturated solutions under controlled high temperature and high pressure condition. The experimental apparatus consists of two vessels for preparation of the Si-supersaturated solution and for precipitation, respectively. The precipitation vessel has double-structure: the main flow path was the inner alumina tube (diameter=4mm), and the outer SUS tube was filled with static solutions. The advantage of this system is that we can take out the non-destructive sample for the X-ray CT analyses. We conducted two types experiments: first one is precipitation in porous media with alumina balls, the second one is rock slice as analog of a fracture.

In the alumina-ball experiments, we carried out the precipitation experiment at supercritical (430C, 30MPa) and vapor condition (370C, 20MPa). In both experiments, the significant silica precipitation within few days, but showed contrasting porosity structures. Under supercritical condition, amorphous silica was predominantly formed with covering the surfaces of the alumina balls and alumina tube, and discrete quartz crystal (50 μm) within the amorphous silica layers. The porosity (ϕ) gradually decreases with minimal porosity ($\phi = 0.4$) at $\sim 38\text{mm}$ from the inlet. In contrast, under vapor condition, fine-grained quartz grains (0.1-1 μm) were directly nucleated in solutions using surface of vapor, and immediately settled on the bottom. The porosity rapidly decreases from 18 mm ($\phi = 0.8$) to 25 mm ($\phi < 0.1$) from the inlet. These results suggest that a depressurization of crustal fluids related to fault dilation by earthquakes would cause a formation of fine-grained silica particles, and their mineralogy and transport/deposition properties strongly depend on properties water.

In the experiment with rock slits, we evaluated the effect of rock substrate (amount and distribution quartz in the fracture wall). The P-T conditions and solution chemistry are similar to the previous experiments, but we used granite core with a slit ($\sim 300 \mu\text{m}$). The mineralogy and aperture structures changes systematically along the fluid flow path. From the inlet to 35 mm of fracture, nucleation of quartz and other silica polymorphs predominantly occurred, regardless of vein wall minerals. From $>35\text{mm}$ low Si concentration, silica precipitates occurred as epitaxial overgrowth from quartz crystal. The wavelength of aperture structures is controlled by distribution and grain size of quartz of the host granite. Accordingly, fractures are not sealed homogeneously, but complex flow pathways are evolved during vein formation. Such a variation in the precipitation mechanism and porosity structures during quartz vein formation may affect the evolutions of permeability and strength of rock fractures in the Earth's crust.

Keywords: Hydrothermal experiments, Quartz, Vein, Fracture, Porosity

High precision in situ Pb isotope analysis of galena by LAL-ICPMS technique

WAKAKI, Shigeyuki^{1*} ; TANIMIZU, Masaharu¹

¹Kochi Institute for Core Sample Research, JAMSTEC

Radiogenic Nd and Pb isotopic compositions of the fluids originated from subducting Pacific and Philippine Sea plates have been characterized from isotopic trends observed among arctic volcanic rocks (Nakamura et al., 2008). Origin and evolution of the fluids that produced hydrothermal ore deposits may now be investigated by radiogenic isotopic compositions of ore deposits. In this study, we analyzed the micro scale isotopic variation of Pb in a hydrothermal galena to shed light on the macro scale dynamics of the fluids. To investigate the possibly small degree of isotopic changes within a galena sample, both high spatial resolution and high precision are required for the isotopic analysis. We employed the combination of laser ablation in liquid (LAL) micro sampling technique (Okabayashi and Hirata, 2011) and solution-based Pb isotopic analysis by MC-ICPMS technique to meet the analytical requirements. In the LAL micro sampling, laser-ablated sample particles are trapped in the liquid that placed above the sampling area. The trapped samples are then dissolved and introduced to the ICPMS as a solution. The advantage of the combined LAL-ICPMS technique over laser ablation (LA) ICPMS technique is the stable ion signals due to solution form, which allows high-precision isotope ratio measurement.

Sample analyzed in this study was a hydrothermal galena from Hosokura mine (Miyagi, Japan). A microscopic texture of the sample was observed in detail with FE-SEM-EDS system (JEOL JSM-6500F) prior to the isotopic analysis. A fs laser (IFRIT, Cyber Laser, Japan) with a wavelength of 780 nm (~200 fs pulse width) was used for the LAL micro sampling. Care was taken to avoid sampling of grain boundaries and inclusions. Typical spatial resolution was 150 micron in diameter and 30 micron in depth. The laser-sampled PbS (300-400ng Pb) trapped in Milli-Q water was dissolved in conc. HNO₃, and adjusted to 200 ng/mL Pb solution in 0.15 M HNO₃ for Pb isotopic analysis. Pb isotope ratios were determined with a MC-ICPMS, Neptune (Thermo Instruments, Bremen, Germany). An isotopic reference material of Tl (NIST-SRM 997) was added to the final sample solutions for the correction of mass discrimination of Pb in the instrument to have a concentration of 20 ppb Tl.

Galena occurs as discrete layers of ca. 1cm width in between layered CaF₂ as well as sub mm-sized inclusion within thick CaF₂ layer. Galena inclusion and layers were numbered from 1 to 3 according to its precipitation order. Grain size of the galena in each of the layer is several hundred microns to several millimeters. Euhedral quartz with a size of 10-100 micron occurs along the grain boundary of galena and as an inclusion within galena grains.

Small but significant Pb isotopic variation of sub-permil order was observed among and within the 3 galena layers. The analyzed samples clearly form a linear trend in the ²⁰⁸Pb/²⁰⁷Pb vs. ²⁰⁶Pb/²⁰⁷Pb diagram. The observed Pb isotopic trend indicates that the Pb isotopic composition of the fluid that produced the galena has slightly changed during galena precipitation. The Pb isotopic composition of the galena is consistent with mixing of a sediment component of the Pacific plate (Nakamura et al., 2008) with a deep fluid derived from Pacific Ocean plate (Nakamura et al., 2008) and/or the DMM. With the high-precision isotopic analysis as demonstrated in this study, LAL-ICPMS may have an important contribution to high-spatial-resolution geochemical studies in the future.

Keywords: Geofluids, laser ablation in liquid, Pb isotope ratio, galena, in situ isotope analysis

Origin of saline waters distributed along the Median Tectonic Line in southwest Japan

AMITA, Kazuhiro^{1*} ; OHSAWA, Shinji² ; NISHIMURA, Koshi³ ; YAMADA, Makoto⁴ ; MISHIMA, Taketoshi² ; KAZAHAYA, Kohei⁵ ; MORIKAWA, Noritoshi⁵ ; HIRAJIMA, Takao⁶

¹Department of Earth Science & Technology Faculty of Engineering and Resource Science Akita University, ²Institute for Geothermal Sciences, Graduate School of Science, Kyoto University, ³Faculty of Economics, Toyo University, ⁴Research Institute for Humanity and Nature, ⁵Geological Survey of Japan, AIST, ⁶Department of Geology and Mineralogy, Graduate School of Science, Kyoto University

To identify of metamorphic dehydrated fluid as source fluid of hot spring water, we conducted chemical and isotopic analyses of water and accompanied gas samples collected from hot-spring wells along the Median Tectonic Line (MTL) in the forearc region of the southwestern part of Japan. As a result, we found hot spring waters having anomalous dD and d¹⁸O compositions as compared with modern seawater and shallow groundwater in Wakayama and Shikoku regions. Judging from data in relative B-Li-Cl composition and He isotopic systematics, the source fluid of the hot springs in Shikoku could be identified to be one of diagenetic fluids. On the other hand, the source fluid of the hot springs of Wakayama had different B-Li-Cl composition and higher 3He/4He ratio in comparison with diagenetic dehydrated fluids and then the fluid was thought to be originated from metamorphic dehydrated fluid as well as Oita plain. There was another striking contrast between the source fluid of Wakayama and Oita and that of Shikoku and Miyazaki; accompanied gases by the former were rich in CO₂, whereas those with the latter were rich in CH₄, and CO₂ in the accompanied gases of Wakayama and Oita is mostly derived from marine carbonate like volcanic gases in subduction zones. Moreover, the Li-B-Cl compositions of them showed transitive values between the relative composition of diagenetic fluids and those of volcanic thermal waters. Consequently, the source fluid of hot springs in Wakayama and Oita was likely to be dehydrated metamorphic fluids released from the subducting Philippine-Sea plate.

Keywords: hot spring water, dehydrated fluid from subducting plate, Median Tectonic Line

Distribution of the helium isotope ratios in northeast Japan in terms of geological setting

HORIGUCHI, Keika^{1*} ; KAZAHAYA, Kohei¹ ; TSUKAMOTO, Hitoshi¹ ; MORIKAWA, Noritoshi¹ ; SATO, Tsutomu¹ ; OHWADA, Michiko¹ ; NAKAMA, Atsuko¹

¹Geological Survey of Japan, AIST

The distribution of slab fluid defined by high Li/Cl ratios conforms the area of "hot fingers" (Tamura et al., 2002) in Northeast Japan (Kazahaya et al., submitted). Conversely, the high $^3\text{He}/^4\text{He}$ ratios distribute wider and do not match with slab-derived fluids indicating that some of the mantle-derived helium would not be transported with magmas or slab fluids but directly upwells as mantle-derived fluid. The $^3\text{He}/^4\text{He}$ ratios vary along the volcanic front showing an areal contrast; such as a low-ratio-area close to volcanoes are observed in the central part of Tohoku. We propose here an extended helium upwell model which can explain the spatial variation of $^3\text{He}/^4\text{He}$ ratios with the following concept; 1) The most important constraint for mantle helium upwelling is the crustal structure divided by tectonic lines; Hatagawa Tectonic Line (HTL) divides the Kitakami and Abukuma belts. Ryoke belt and north part of Abukuma belt is torn apart by number of faulting events. The rest of parts, Abukuma granitic province and Kitakami province form very large stable blocks which might prohibit helium to upwell from mantle. 2) A view from U-Th content in the crust is important to understand the flat distribution of mantle helium in back-arc region; Low U-Th crust in the back-arc with less crustal ^4He production is favorable to explain the flat and high $^3\text{He}/^4\text{He}$ signature, such as oceanic crust might have. Tanakura Tectonic Line (TTL) divides the thick crust of continental margin (sedimentary prism and granite) with Ryoke belt.

Keywords: helium isotope ratio, northeast Japan, areal distribution, geological structure

The Li-Cl-Br systematics of saline groundwater: A new indicator for slab fluid

KAZAHAYA, Kohei^{1*}; TAKAHASHI, Masaaki¹; IWAMORI, Hikaru²

¹Geological Survey of Japan, AIST, ²Geochemical Evolution Research Program, Japan Agency for Marine-Earth Science and Technology

In this study, we propose Br/Cl ratio as a new indicator for slab-derived fluids, which is useful to distinguish their sources between pore water and hydrous minerals in subducting slab. The areal distribution of slab-derived fluids and their sources using Li/Cl and Br/Cl as geochemical evidences will provide a view for water circulation in subduction zones.

Subducting slab contains waters (originally seawater) as pore water and many kinds of hydrous minerals. Hydrous minerals such as opal, clay or mica will decompose to release water during subsiding, and pore water will be released by compaction. Even though such complex process occurs, behavior of halogen ions in the subducting slab may be simple because they are always enriched in aqueous phase (pore water) and the rest are in minerals as a replacement of OH. Some metamorphic fluids in wedge mantle peridotite with Br-enriched signature have been observed and were indicated to be from pore water in the slab. The mineral dehydration process is supposed to be responsible for Br-depletion in slab-derived aqueous fluid. Therefore, halogens are potentially good indicators concerning with the water behavior in subduction processes.

The higher Br/Cl ratios (>0.0035 in wt.) have been observed in fossil seawater and oil field brines due to the addition of Br from organic matters. The very low Br/Cl waters (<0.0025 in wt.) have feature of ¹⁸O-shift to the slab (magmatic) fluid end member, which is quite lower than that in seawater (Br/Cl = 0.0034 in wt.), indicating that these waters originate from dehydration of the slab.

Keywords: Li-Cl-Br, slab-derived fluid, groundwater, subduction process

Origin of U-Th disequilibrium in subduction zone volcanic rocks

YOKOYAMA, Tetsuya^{1*}; IKEMOTO, Akihiko¹; IWAMORI, Hikaru²; UEKI, Kenta¹

¹Department of Earth and Planetary Sciences, Tokyo Institute of Technology, ²JAMSTEC

Subduction zone magmatism is induced by the addition of slab derived fluids to the mantle wedge [1]. Chemical compositions of subduction zone volcanic rocks are largely controlled by the chemical and physical properties of the slab fluid. The nature of slab fluids have been extensively studied by geochemical approach utilizing trace element abundances and isotope compositions in arc basalts [2]. U-series disequilibrium in arc volcanic rocks is a useful tracer to understand the origin of arc magmas as well as the timescales of fluid/melt migration in subduction zones. However, detail of the process that producing ²³⁸U-²³⁰Th disequilibrium in primary melts in the mantle wedge is still poorly constrained.

In this study, we determined ²³⁸U-²³⁰Th disequilibrium in volcanic rocks from the Northeast Japan Arc (Iwate, Akitakoma, Yakeyama, Hachimantai, and Kampu). In addition, we performed a numerical simulation that reproduced (²³⁸U/²³²Th) and (²³⁰Th/²³²Th) ratios in primary melts in a subduction zone, by simultaneously calculating mantle dynamics, hydro phase reactions and trace elements transport. To discuss the origin of U-Th disequilibrium in arc volcanic rocks, the new data and previously published U-Th data around Japan were evaluated based on the result of the numerical simulation. The numerical simulation performed in this study

Most of arc volcanic rocks possess ²³⁸U-²³⁰Th disequilibrium with ²³⁸U excesses, suggesting the addition to the mantle wedge of slab fluid enriched in U relative to Th. The feature of ²³⁸U enrichment is well reproduced by the numerical simulation. Interestingly, the simulation produced two positive trends in the U-Th diagram; the shallow trend matches data from the Izu-Mariana arc, while the steep slope is consistent with data from the Kamchatka arc. This strongly suggests that the positive trend in the U-Th diagram for a single arc samples simply reflects the variation of (²³⁸U/²³²Th) and (²³⁰Th/²³²Th) ratios in primary melts produced in the mantle wedge, and the slope does not have any age significance. Thus, as discussed in [3], the decoupling of U-Th and Th-Ra ages for arc samples would be explained by assuming that the slab derived fluid have (²³⁰Th/²³²Th) ratios higher than the mantle wedge composition.

Although the NEJ frontal-arc lavas (Iwate) possess ²³⁸U-²³⁰Th disequilibrium with ²³⁸U excesses, the extent of ²³⁸U enrichment is moderate (<10%) compared to the other frontal-arc samples. In addition, Iwate lavas have relatively low (²³⁰Th/²³²Th) ratios that cannot be explained by the numerical simulation. This implies that the (²³⁰Th/²³²Th) in mantle wedge beneath Iwate volcano is lower than that in the depleted MORB mantle (DMM), due presumably to ancient mantle metasomatism by Th-enriched fluids derived from sediments.

In contrast to the frontal arc samples, the extent of ²³⁸U enrichment in the NEJ samples decreases as the slab depth increases, and the rear-arc lavas (Kampu) show ²³⁰Th enrichments relative to ²³⁸U (<10%). This generally reflects gradual decrease of the amount of slab derived fluid mixed into the wedge mantle. The ²³⁰Th excesses in rear-arc lavas would be produced by the melting of garnet-bearing upwelling mantle, as reproduced by the simulation. However, our data for Kampu show ²³⁰Th excesses with an extremely low (²³⁰Th/²³²Th) ratio (~0.8) that plots outside the simulation data. This is explained by assuming the existence of metasomatised mantle beneath the NE Japan as discussed above, although the possibility of direct addition of Th-enriched fluid to the DMM-like mantle cannot be ruled out for the generation of rear-arc magmas.

References: [1] Iwamori (1998) *EPSL* 160, 65. [2] Nakamura et al. (2008) *Nature Geosci.* 1 380. [3] Yokoyama et al. (2003) *JGR* doi: 10.1029/2002JB002103.

Keywords: U-Th disequilibrium, Subduction zone, volcanic rocks, slab derived fluid

Water transport coupled dynamically with a plate-mantle convection system involving a shallow to deep subduction zone

NAKAKUKI, Tomoeki^{1*}; KANEKO, Takeo¹; NAKAO, Atsushi²; IWAMORI, Hikaru³

¹Dept. Earth and Planetary Systems Science, Hiroshima Univ., ²Dept. Earth and Planetary Sciences, Tokyo Inst. Technology, ³Geochemical Evolution Research Program, JAMSTEC

Numerical study for water transport under a volcanic arc revealed dynamics of the water processes inducing melt generation (Iwamori, 1998; 2007). Back-arc and intra-plate volcanisms also indicate water migration from a deeper section of the subduction zone. Aiming to understand geodynamical processes of water derived and transported from the subducted slab in the deep subduction zone, we developed a numerical model of water transport coupled dynamically with plate-mantle convection system with a whole mantle scale. We here focus on the mechanism of dehydration from stagnating or penetrating slab and water transport from the mantle transition zone (MTZ). We also consider water transport to deeper mantle and the effects on the global distribution of water-compatible elements (Iwamori and Nakamura, 2012).

We assume that a viscous fluid in a 2-D rectangular box with an extended Boussinesq approximation represents the mantle convection system with integrated lithospheric plates (Tagawa et al, 2007). We incorporate water transport and hydrous mineral phase diagram (Iwamori, 1998; 2007) into the numerical plate-mantle model. We assume that the water dehydrated from water-saturated minerals migrates upward with porous flow that is much faster than mantle flow. In our model, the emitted water is instantaneously transported only to the upward direction. We introduce reduction of the density and the viscosity due to the hydration into the density and rheology model according to experimental study (karato and Jung, 2003). We also consider viscous weakening of serpentine or chlorite that is important for water transport in shallow subduction zone [6]. A numerical method developed by Tagawa et al. (2007) is used to solve momentum and energy conservation equations for the mantle convection. To solve an equation for water transport advected by the mantle flow in which the diffusion term is negligible, a Marker-And-Cell (MAC) method is employed to avoid artificial diffusion.

A serpentine layer generated by dehydration of the oceanic crust plays a key role to control water transport by the subducted slab shallower than about 150 km (Iwamori, 1998; 2007; Horiuchi, 2013). To continuously generate this layer, coupling between the serpentine layer and the plate boundary fault is essential. After dehydration of serpentine, nominally anhydrous minerals (NAMs) (Iwamori, 1998; 2007) are a main veneer of the water. In this stage, water capacity of NAMs, which depends on the grain boundary storage as well as that of the hydrous minerals, is the primary factor to control the amount of transported water. This is not so large as about 0.4 wt. % to maintain water-filled region under the arc. The water is carried without dehydration above the 660 km boundary. If the water capacity in the lower mantle is as large as that of NAMs in the mantle shallower than 410 km (~0.2 wt. %), the water is entirely transported to the lower mantle. When the lower mantle water capacity is lower than that, the water is expelled at the post-spinel phase transition. While the water ascends with the porous flow, the medium rocks descend with asthenospheric flow dragged by the downwelling slab. The repetition of these processes broadens the hydrous layer at the 660 km boundary. A thin water-saturated layer is formed at the 660 km boundary around the penetrating slab. Because of the buoyancy, this becomes unstable so that hydrous plumes are generated. On the contrary to this, the hydrous plume was not formed from the hydrous NAMs layer over the stagnant slab. At the 410 km boundary, the water is ejected from the hydrous plume as the olivine phase minerals can bear the water much less than MTZ minerals. The ejected water rises with porous flow till the emission is completed. The hydrous plumes fill the water within the mantle wedge from the edge to the 500 to 1000 km distant back-arc area, and those erode to thin the overriding lithosphere.

Keywords: subduction zone, water transport, transition zone, slab, hydrous plume, mantle convection

An overview of seismic coupling and crustal deformation on the basis of geofluid and shallow slow earthquakes

ARIYOSHI, Keisuke^{1*}; MATSUZAWA, Toru²; HINO, Ryota³; HASEGAWA, Akira²; HORI, Takane¹; NAKATA, Ryoko¹; KANEDA, Yoshiyuki¹

¹Japan Agency for Marine-Earth Science and Technology (JAMSTEC), ²Research Center for Prediction of Earthquakes and Volcanic Eruptions, Tohoku University, ³International Research Institute of Disaster Science, Tohoku University

Due to the use of broadband seafloor seismometers near the trench and dense inland networks of highly sensitive seismic stations, very low-frequency events (VLFs) have been observed in the shallow transition zone near the trench of subduction plate boundaries as well as the deep one. Following the 2004 Sumatra Earthquake, the Japanese government has established the Dense Oceanfloor Network system for Earthquakes and Tsunamis (DONET) along the Nankai Trough. In the Tonankai district, M8-class megathrust earthquakes will probably occur in the near future; DONET-I has now operated since August 2011. In this study, we perform numerical simulations of multiscale earthquake cycles, including a megathrust earthquake and VLFs, on a 3-D subduction plate boundary, in order to understand the change in VLF activity after megathrust earthquakes and hydraulic pressure gauge data.

In our simulation, the motion equation for a subduction plate boundary is described by a quasi-dynamic equilibrium between the shear stress (due to reverse dip-slip on the discretized faults) and the frictional stress based on a rate- and state-dependent friction (RSF) law. To perform multiscale earthquake cycle simulations, we assumed single large asperity and numerous small asperities arranged along the strike direction, where the large asperity generates megathrust earthquakes and a chain reaction of numerous small asperities generate a migration of slow earthquakes along the strike direction.

From our simulation results, we concluded as follows: (i) For a megathrust earthquake in which the coseismic slip penetrates to the trench, plate coupling in the postseismic stage will be strong in the region from the central part of the source region to the shallower part toward the trench, which will cause the shallow VLF after-events to be quiescent or to occur infrequently in isolation. On the outer rim, shallow VLF after-events will be reactivated earlier than they will be in the center because of weak plate coupling. (ii) Since leveling change due to slow earthquakes at DONET is expected to be local and incoherent in the same node because of the short distance between their sources and the (DONET) receiver, it is useful to remove an average from original data in the same node in order to extract a signal.

Keywords: megathrust earthquake, subduction zone, seismic quiescence, high pore pressure, seafloor observation, rate- and state-dependent friction law

Three-dimensional seismic attenuation structure beneath Kyusyu

SAITA, Hiroto^{1*} ; NAKAJIMA, Junichi¹

¹Tohoku University

The Philippine Sea (PHS) plate is subducting beneath Kyusyu and a clear volcanic front is formed through the middle of the arc. Furthermore, there is a volcanic gap between Aso and Kirishima volcanos. Seismic attenuation provides additional insights into subduction-zone dynamics, because higher-temperature environments or the existence of fluids may have different effects on seismic attenuation from on seismic velocity. Therefore the estimate of seismic attenuation is very important to understand arc magmatism and mantle dynamics in subduction zone. This study estimates seismic attenuation structure beneath Kyushu using a large number of high-quality waveform data. Data and method

We used 5195 earthquakes that occurred from April 2003 to December 2013 by applying the method of Nakajima et al. [2013] to waveform data recorded at a nation-wide seismograph network in Japan. We determined the corner frequency of earthquakes by using the spectral ratio method of S-coda waves. Then, we determined a whole-path attenuation term (t^*), site-amplification factors and spectrum level simultaneously by a joint inversion. Finally, these t^* values ($N= 75207$) were inverted to obtain three-dimensional attenuation structure.

The obtained results show several interesting feature. First, the subducting PHS slab is imaged as a low attenuation zone. Second, an inclined high-attenuation zone that is interpreted as mantle upwelling flow is served in the back-arc mantle. However, the inclined high-attenuation zone is less developed in the volcanic gap between Aso and Kirishima volcanos. This correspondence suggests the important role of mantle-wedge processes in the genesis of arc magmas.

Keywords: seismic attenuation structure, Philippine Sea Plate, Kyusyu

3D Electrical Resistivity Imaging beneath Kyushu by Geomagnetic transfer function data

HATA, Maki^{1*}; UYESHIMA, Makoto¹; HANDA, Shun²; SHIMOIZUMI, Masashi³; TANAKA, Yoshikazu⁴; HASHIMOTO, Takeshi⁵; KAGIYAMA, Tsuneomi⁴; UTADA, Hisashi¹; MUNEKANE, Hiroshi⁶; ICHIKI, Masahiro⁷; FUJI-TA, Kiyoshi⁸

¹Earthquake Research Institute, the University of Tokyo, ²Faculty of Agricultural Science, Saga University, ³Kyushu Polytechnic College, ⁴Graduate School of Science, Kyoto University, ⁵Institute of Seismology and Volcanology, Graduate School of Science, Hokkaido University, ⁶Geographical Survey Institute, ⁷Graduate School of Science, Tohoku University, ⁸GSE, Osaka University

The Kyushu island in the Southwest Japan Arc has many Quaternary active volcanoes in relation to the subduction of the Philippine Sea Plate (PSP). The volcanoes exist along the volcanic front of N30°E-S30°W, whereas the volcanoes are densely located in the northern and southern regions of the island. The Kyushu island has a non-volcanic region in the central region of the island between the two volcanic regions. We performed three-dimensional (3D) inversion analyses to obtain a lithospheric-scale electrical resistivity model beneath the entire Kyushu island using the Network-Magnetotelluric (MT) data. The electrical resistivity model, however, has a limited resolution in a horizontal direction because of the sparse Network-MT data in several areas of Kyushu. Thus data of geomagnetic variations are used anew to improve the uncertainty of the electrical resistivity structure in a horizontal direction. Data of geomagnetic variations were obtained at the entire Kyushu island and several islands off the western coast of Kyushu from 1980's to 1990's [e.g., Handa et al., 1992; Shimoizumi et al., 1997; Munekane et al., 1997]. In this study, accessible data of geomagnetic variations around Kyushu are compiled. Geomagnetic transfer functions for the data of geomagnetic variations in the northern Kyushu are re-estimated using the BIRRP code [Chave and Thomson, 2004] in order to enhance the quality of the transfer functions and their error estimation. The transfer functions at about 150 sites, which are 12 periods between 20 and 960 s, are obtained with improving quality at the entire Kyushu island. The induction vector representation [Parkinson, 1962] is generally used to delineate the lateral variation of electrical resistivity structure because the vectors point to current concentration in conductive anomalies. Induction vectors determined using the improved transfer functions have the following specific features. First, the vectors on the northern and central Kyushu do not point to the Pacific ocean off the eastern coast of Kyushu but point to the East China Sea of the shallow sea off the western coast of Kyushu. Second, the induction vectors on the southern Kyushu point to the Pacific ocean in the eastern part and point to the East China Sea in the western part at short period, whereas the vectors are arranged along a direction parallel to a direction of the coast line at longer period (>300 s). These results are consistent with the previous work [Handa et al., 1992; Shimoizumi et al., 1997; Munekane, 2000]. It is considered that the complex behavior of the induction vectors are influenced by conditions of the Earth's mantle relating to the igneous activities. Then we applied three-dimensional (3D) inversion analyses for geomagnetic transfer functions using the WSINV3DMT inversion code [Siripunvaraporn and Egbert, 2009]. The electrical resistivity of a starting model is based on values of the 3D electrical resistivity model estimated by using the Network-MT data. In this presentation, we will mainly describe features of the 3D electrical resistivity structure using the geomagnetic transfer functions and them of the 3D electrical resistivity structure using only the Network-MT data [Hata et al., 2013].

Influence of confining and pore-fluid pressures on velocity and conductivity of a fluid-saturated rock

SEMA, Fumie^{1*} ; MAKIMURA, Miho¹ ; HIGUCHI, Akiyoshi¹ ; WATANABE, Tohru¹

¹Department of Earth Sciences, University of Toyama

Pore-fluid pressure in seismogenic zones can play a key role in the occurrence of an earthquake (e.g., Sibson, 2009). Its evaluation via geophysical observation can lead to a good understanding of seismic activities. It is critical to understand how pore-fluid pressure affects seismic velocity and electrical conductivity. We have studied the influence of pore-fluid pressure on elastic wave velocity and electrical conductivity of water-saturated rocks.

Measurements have been made using a 200 MPa hydrostatic pressure vessel, in which confining and pore-fluid pressures can be separately controlled. An aqueous pore-fluid is electrically insulated from the metal work by using a specially designed device (Watanabe and Higuchi, 2013). Elastic wave velocity was measured with the pulse transmission technique (PZT transducers, $f=2$ MHz), and electrical conductivity the four-electrode method (Ag-AgCl electrodes, $f=100$ mHz-100 kHz) to minimize the influence of polarization on electrodes.

Berea sandstone (OH, USA) was used for its high porosity (19.1%) and permeability ($\sim 10^{-13}$ m²). It is mainly composed of subangular quartz grains. Microstructural examinations show clay minerals (e.g., kaolinite) and carbonates (e.g., calcite) fill many gaps between quartz grains. A small amount of feldspar grains are also present. The grain size is 100-200 micrometers. Cylindrical samples have dimensions of 25 mm in diameter and 30 mm in length. Their axes are perpendicular to sedimentation bed. Elastic wave velocity is slightly higher in the direction perpendicular to the axis than in that parallel to the axis.

Confining and pore-fluid pressures work in opposite ways. Increasing confining pressure closes pores, while increasing pore-fluid pressure opens them. For a given pore-fluid pressure, both compressional and shear velocities increase with increasing confining pressure, while electrical conductivity decreases. When confining pressure is fixed, velocity decreases with increasing pore-fluid pressure while conductivity increases. The closure and opening of pores can explain observed changes of velocity and conductivity.

Effective confining pressure is defined by the difference between confining and pore-fluid pressures. Velocity increases with increasing effective confining pressure, while conductivity decreases. However, neither velocity nor conductivity is unique function of the effective confining pressure. For a given effective confining pressure, conductivity significantly increases with increasing confining pressure. Velocity also increases with increasing confining pressure, though it is not so significant. Increasing pore-fluid pressure can compress clay minerals to increase pore space. This might explain observed conductivity change.

Keywords: pore-fluid pressure, seismic velocity, electrical conductivity, geofluid

A study on grain boundary brine in halite rocks using electrical conductivity measurements

WATANABE, Tohru^{1*} ; KITANO, Motoki¹

¹Graduate school of science and engineering, University of Toyama

Intercrystalline fluid can significantly affect rheological and transport properties of rocks. Its influences are strongly dependent on the style of distribution. When a fluid fills grain boundaries in a rock, it will significantly reduce the strength of the rock. The fluid distribution is mainly controlled by the dihedral angle between solid and fluid phases. The grain boundary wetting is expected only when the dihedral angle is 0°. The dihedral angle of the halite-water system was studied through microstructural analyses of quenched materials (Lewis and Holness, 1996). The dihedral angle is 50~70° at $P < 200$ MPa and $T < 300$ °C. However, deformation experiments (e.g., Watanabe and Peach, 2002) and cryo-SEM observations (e.g., Schenk et al., 2006) on halite rocks have indicated the coexistence of grain boundary brine with a positive dihedral angle. In order to understand the nature of grain boundary brine, we have conducted electrical impedance measurements on synthetic wet halite rocks over a wide range of pressure and temperature.

Wet halite rock samples (9 mm diameter and 6 mm long) are prepared by cold-pressing ($P=140$ MPa, 40 min.) of wet NaCl powder and annealing ($T=180$ °C, $P=180$ MPa, 160 hours). Grains are polygonal and equidimensional with a mean diameter of 50-100 μ m. The porosity is less than 1 %. The volume fraction of brine is estimated to be 11.1% by the thermo gravimetric analysis. Microstructural observation shows that most of brine is enclosed inside halite grains. Electrical impedance is measured in the axial direction of a sample by a lock-in-amplifier (SRS, SR830) with a current amplifier (SRS, SR570). The cylindrical surface of a sample is weakly dried and coated with RTV rubber to suppress the contribution of surface conduction. A conventional externally heated, cold-seal vessel (pressure medium: silicone oil) is used to control pressure and temperature.

Electrical conductivity of wet halite rocks is higher than that of NaCl by orders of magnitude even at the conditions of the dihedral angle larger than 60 degrees. The conduction through brine dominates the bulk conduction. This is also supported by the quick conductivity change in response to the change in pressure. Brine is interconnected over a whole range of pressure and temperature.

No remarkable change in conductivity is observed around the condition of the dihedral angle of 60 degrees. Although the interconnection of triple-junction tubes might drastically change at the dihedral angle of 60 degrees, its influence on the bulk conductivity is masked by more conductive paths. A triple-junction tube is so stiff that it cannot give observed conductivity changes in response to changes in pressure. The dominant conduction paths are not triple-junction tubes. Grain boundary brine must be the dominant conduction paths.

Electrical conductivity decreases with increasing pressure. Larger change is observed for lower temperatures. A simple model of fluid tube with elliptical cross-section shows that the thickness of a fluid tube decreases by less than 10%. The observed large change in conductivity suggests that the conductivity of brine is strongly dependent on the fluid thickness. When the thickness is comparable to the molecular size, the mobility of ions must be sensitive to the thickness. The observed large change in conductivity might be caused by the decrease in ionic mobility.

Keywords: salt, grain boundary, water, electrical conductivity

Estimation of the maximum burial depth of siltstones from the Kazusa Group by laboratory experiments

TAMURA, Yukie¹ ; MARUMO, Haruna² ; MITSUHASHI, Shunsuke¹ ; UEHARA, Shin-ichi^{1*}

¹Faculty of Science, Toho University, ²Graduate School of Science, Toho University

To evaluate maximum burial depth of sedimentary formations is important for many topics in earth science and engineering such as estimating uplift and erosion of sedimentary basins. As a one of effective methods of the evaluation, a laboratory-based method for determining the maximum effective stress have been proposed. This method is based on a conventional method to evaluate preconsolidation stress (maximum effective stress experienced) of soil. However, this method cannot be necessarily applied to sedimentary rocks in simple ways, because sedimentary rocks have experienced not only mechanical compaction but also other processes such as cementation between grains, which should affect the mechanical properties of the rock. Thus applicability of this method to sedimentary rocks should be examined for several sedimentary basins. We performed laboratory experiments to measure porosity of siltstone specimens collected from several formations of the Kazusa Group, Boso peninsula, Japan, and tried to estimate the maximum burial depth based the results. We then compared the results with differences of burial depth ($\Delta Depth$) among locations of collecting samples which were estimated from geological setting, and examined the applicability of this method for estimation of the maximum burial depth in this site.

We collected rock blocks from Umegase (UMG), Otadai (OTD), Kiwada (KWD), Ohara (OHR), and Katsuura (KTR) Formations (in the descending order of stratigraphic horizon), and prepared cylindrical specimens of approximately 40 mm in diameter and 30 mm in length from these blocks. The porosity of these specimens was measured under different confining pressure (up to 35 MPa) and constant pore pressure (1 MPa) by using an intra-vessel deformation fluid-flow apparatus at Toho University. We used water as a pore fluid, and the measurements were performed at room temperature. Porosity under each effective pressure (the difference between confining pressure and pore pressure) was estimated by measuring volume of water drained from a specimen when confining pressure was loaded. The relation between measured porosity and effective pressure could be bilinear in log-log scale. The maximum effective stress experienced ($P_{e,B}$) of the tested rocks was determined from the intersection point of the two straight lines of the compaction curve. The maximum burial depth (D_{max}) was obtained by $D_{max} = P_{e,B} / [(\rho_r - \rho_w)g]$, where ρ_r , ρ_w and g are density of rock, water and gravity acceleration, respectively.

In the case of UMG, OTD and KTR, porosities decrease as the burial depth increases. Porosities of OHR and KWD, however, were relatively high although their burial depth is relatively large. There was a linear correlation between D_{max} and $\Delta Depth$ except for OHR, but the slope of the relationship was less than one (approximately 0.27). Therefore, further investigation is necessary to examine the applicability of this methods to this site. $P_{e,B}$ of OHR was less than that of other specimens, which supports the possibility that pore pressure in this formation was approximately 5 to 12 MPa higher than hydrostatic conditions.

Keywords: porosity, maximum burial depth, maximum effective stress experienced, Kazusa Group, overpressure, laboratory rock experiment

Experimental constraints on the serpentinization rate under the antigorite-stable P-T condition

NAKATANI, Takayuki^{1*} ; NAKAMURA, Michihiko¹

¹Earth and Planet Materials Sci., Tohoku Univ.

Water transport into the Earth's interior can be limited by the rate of serpentinization reaction proceeding at slow spreading ridges and along bending related faults (Iyer et al., 2012). Moreover, the distribution of H₂O in the mantle wedge may be controlled by the extent of progression of the reaction between the slab-derived fluid and the hanging wall mantle, as suggested by theoretical models (Iwamori, 1998). Previous hydration experiments for kinetic studies have been vigorously conducted at relatively low P-T condition (up to ca. 400 °C and 0.3 GPa) where the low T serpentine variety lizardite or chrysotile is stable. In contrast, antigorite is expected to be the dominant serpentine variety under the higher P-T condition corresponding to the deep oceanic lithosphere and the mantle wedge.

In order to constrain the serpentinization rates of peridotite under the antigorite-stable conditions, we conducted piston-cylinder experiments at 580 °C and 1.3 GPa. Four types of starting materials were prepared from the crushed powder of a San Carlos lherzolite xenolith: 1) olivine (Ol), 2) orthopyroxene (Opx) + clinopyroxene (Cpx), 3) Ol + Opx, and 4) Ol + Opx + Cpx + spinel. These systems were abbreviated as OL, OPX+CPX, OL+OPX, and LHZ, respectively. The starting materials were reacted with 15 wt% distilled water for 4-15 days. The formation of serpentine + talc + magnetite was observed in all the systems except for OL. Based on Raman spectroscopy results and crystal shapes, the synthesized serpentine mineral was identified as lizardite with 6.9 wt% Al₂O₃, rather than antigorite. The high Al₂O₃ content in the system possibly stabilized the aluminous lizardite at the experimental temperatures. Low silica activity precluded olivine reaction in the OL system, whereas olivine reacted with the SiO₂ component in orthopyroxene to form lizardite and talc in the other systems. The reaction progress followed an interface-controlled rate law. The growth rate, *G*, was estimated to be 2.31 ± 0.37 , 1.23 ± 0.20 , and 2.78 ± 0.64 μm/day in the OPX+CPX, OL+OPX, and LHZ systems, respectively. As an example, we applied the hydration rates of peridotites, which were obtained experimentally, to a reactive-transport model for the convecting mantle wedge hydration. In the case of grain-scale pervasive flow, the mass flux ratio of water fixable in the hanging wall peridotites to that supplied from the dehydrating oceanic lithosphere was calculated to be $2.7 \times 10^5 - 1.5 \times 10^8$. This indicates that the water is completely fixable in the convecting mantle wedge and carried down to the stability limit of serpentine as soon as it is supplied from the slab. Aqueous fluid may penetrate all the way through the serpentine stable layer and reach the hot center of the mantle wedge only when the fluid migrates via crack-like pathways with a spacing >270-15000 m, which is not consistent with observations of natural serpentinites.

Keywords: hydration, serpentine, fluid, subduction zone, mantle wedge

Diffusive kinetic isotope fractionation of water in silicate glasses

KURODA, Minami^{1*} ; YAMAMOTO, Daiki¹ ; TACHIBANA, Shogo¹ ; NAKAMURA, Michihiko² ; OKUMURA, Satoshi² ; ASAKI, Miho² ; ISHIBASHI, Atsuko¹ ; SAKAMOTO, Naoya¹ ; YURIMOTO, Hisayoshi¹

¹Department of Natural History Science, Hokkaido University, ²Department of Earth Science, Tohoku University

Oversaturation of dissolved volatiles in an ascending magma leads to bubble nucleation and growth, which depend on volatile solubility and diffusivity, and drives explosive volcanic eruptions in the Earth. It is thus important to clarify the behaviors of volatiles in silicate melts in understanding the mechanism and dynamics of volcanic eruptions.

Hydrogen isotopes record the degassing processes of hydrous magmas due to isotopic fractionation between dissolved and exsolved water. The degree of hydrogen isotopic fractionation is correlated with the water content in natural volcanic rock samples; Deuterium is more deficient in water-poor samples, and the degree of D-deficiency increases as the water content decreases. This trend has been interpreted to reflect the transition of degassing model from that in a closed-system to in an open-system. However, these two extreme degassing schemes do not take the diffusive transport of water in magmas into account, which should be included in a realistic degassing model, because the timescale of diffusion is not necessarily negligibly small compared to that of degassing during magma ascent. Moreover, diffusion of water in silicate melts may cause kinetic isotope fractionation between silicate melt and explosive fluid phases because H₂O is likely to diffuse faster than HDO, of which effect can be overprinted in the D/H ratios of natural samples. The hydrogen isotopic fractionation during water diffusion in silicate melts, however, has not yet been fully determined. In order to determine the isotopic fractionation factor of hydrogen due to water diffusion in silicate melts, we performed diffusion experiments of water in SiO₂ and synthetic rhyolite glasses in a D-enriched system (H/D=10, 5 and 1).

The experiments were performed for SiO₂ and rhyolite glasses at 850 °C and water pressure of 50 bar in sealed silica tubes and at 650 °C and water pressure of 500 and 1000 bar in a hydrothermal furnace developed at Tohoku University. Concentration profiles of H and D in run products were measured with the ion microprobe (Cameca ims-6f at Hokkaido University) to evaluate diffusion coefficients of water (including H₂O and HDO) in glasses. The obtained diffusivity (a diffusion coefficient divided by a water content) in SiO₂ glass at 650 and 850 °C were consistent with the values reported in previous studies (Davis and Tomozawa, 1995; Berger and Tomozawa, 2003). The D/H ratios along the diffusion profile were also analyzed for SiO₂ glasses with the ion microprobe. The D/H ratio first decreases, but apparently increases along the profile. The decrease of D/H ratio may imply the kinetic isotope fractionation during diffusion. However, the increase of D/H ratio cannot be explained simply by diffusion and may reflect the change of instrumental mass fractionation with water content (Hauri et al., 2006), which should be precisely determined to correct the profile of hydrogen isotopic ratio.

Keywords: eruption dynamics, silicate glass, water, diffusion, hydrogen isotope, isotopic fractionation

Development of high-precision geobarometer

TAKAHATA, Kohei^{1*} ; TORIMOTO, Junji² ; YAMAMOTO, Junji²

¹Earth and Planetary System Science, Hokkaido University, ²Hokkaido University Museum

Fluid inclusions in mantle-derived minerals can serve as a messenger from deep Earth. If CO₂ is a dominant phase of the fluid, the relationship between intensity ratio and frequency separation of the Fermi diad bands in the Raman spectra of CO₂ can be used for determination of density of the inclusions.

In this study, we installed new Raman spectrometer that was improved spectral resolution. And we also measured its precision of frequency separation (Δ). As a result of this study, we determined that the error of Δ is $\pm 0.003 \text{ cm}^{-1}$ (1σ). Converted into the error of density, this value is $\pm 0.0025 \text{ g / cm}^{-3}$.

Keywords: fluid inclusion, carbon dioxide, Raman spectroscopy, mantle xenolith, geobarometer

Applications of rapid and precise $^{11}\text{B}/^{10}\text{B}$ isotopic analysis to water and rock samples

TANIMIZU, Masaharu^{1*}; NAGAISHI, Kazuya²; ISHIKAWA, Tsuyoshi¹

¹Kochi Institute, JAMSTEC, ²Marine Works Japan Ltd.

Boron isotope ratio is a powerful tracer in the fields of geochemistry, biochemistry, and environmental chemistry. Boron isotope ratios are determined by TIMS or MC-ICP-MS with precisions of better than 0.1 % RSD, but a large inter-lab discrepancy of 0.6 % is still observed for actual carbonate samples (Foster, 2008). Here, we are trying to determine B isotope ratio by MC-ICP-MS with a simple and common analytical techniques using a quartz sample introduction system with a PFA nebulizer, and compared to recently developed precise B isotope ratio analysis techniques by TIMS in positive ion detection mode determined as Cs_2BO_2^+ ions with sample amount of <100 ng (Ishikawa and Nagaishi, 2011) and by MC-ICP-MS (Foster, 2008, Louvat et al., 2011).

In this year, our developed B analytical method above for carbonate and water samples are applied to rock samples. Resultant analytical reproducibility (twice standard deviation) was ± 0.04 % with a consumption of 50 ng B for several geochemical reference rocks issued from GSJ. Their relative differences from the standard were consistent with those determined by the positive TIMS within analytical uncertainty. Current potential B isotopic analysis by MC-ICP-MS will be discussed.

Water migration with a subducting slab and the dynamic effects on whole mantle convection

KANEKO, Takeo^{1*} ; NAKAKUKI, Tomoeiki¹ ; IWAMORI, Hikaru²

¹Dept. Earth and Planetary Systems Science, Hiroshima Univ, ²Geochemical Evolution Research Program, JAMSTEC

Existence of liquid water is a characteristic of the earth. The water of interior of the Earths involved with the subducting plate reduces density and viscosity of the crustal and mantle rocks. These effects are essential to emerge the solid Earth activity such as, plate tectonics and island arc volcanism. Although the most of subducted water circulates through upper mantle, there is a possibility that portion of the water penetrates into lower mantle. Where does the water migrate? How much does the water affect mantle dynamics through the rock rheology and property? We performed numerical mantle convection simulation to investigate the water cycle and dynamic effects on the whole mantle convection.

In this study, we use the numerical model based on the model (Tagawa et al., 2007; Nakakuki et al., 2010) including the subducting oceanic plate driven dynamically. This model includes migration of water with the plate motion. We consider influences of reducing density and viscosity due to the water on the mantle flow (Karato and Jung, 2003). The maximum water content in the upper mantle is determined using phase relations of the basalt and the peridotite (Iwamori, 2004; 2007). We use various values of the maximum water content of rocks in the lower mantle, because it has been not clearly defined. We also treated the following physical properties as varying parameters: friction coefficient at the plate boundary, amount of the water injection at the trench, density-water dependence coefficient, and maximum water content in the lower mantle. Addition to we calculated dislocation creep by non-newtonian fluid or newtonian fluid.

A part of subducted water associate with the subducting oceanic plate is absorbed into peridotitic rocks and transported to about 150 km deep mantle. After that, dehydration with the serpentine decomposition occurs, and transported to deeper mantle by hot nominally anhydrous minerals (NAMs). The amount of dehydration at the 660 km phase boundary depends on the maximum water content of lower mantle, when the slab penetrates into lower mantle. The ejected water forms thin and high-water-content layer over the 660 km phase transition. As a result, the buoyancy of this layer induces instability, so that hydrated plumes are generated. We propose that this mechanism is important for the water cycle in the upper mantle. On the other hand, considerable portion of the water is transported into lower mantle with subducting slab, although notable water capacity of the lower mantle much smaller than that of the upper mantle, and reach core-mantle boundary. We have not yet observed notable water influence on mantle convection at lowermost mantle because of the small water concentration. Also, the hydrated materials do not rise to surface with hot plumes generated at the core-mantle boundary.

Keywords: mantle convection, plume, transition zone, water transport